On the East Australian Current: Variability, Encroachment and Upwelling.

Moninya Roughan*
Scripps Institution of Oceanography, UCSD, La Jolla, CA, USA.
and Jason H. Middleton
School of Mathematics, University of New South Wales, Sydney, Australia.

Submitted to the Journal of Geophysical Research: 21 February 2003

Reference: *J. Geophys. Res.*, *109*(C07003), doi:10.1029/2003JC001833.

Corresponding author address: Moninya Roughan, Scripps Institution of Oceanography, UCSD, 9500 Gilman Drive, La Jolla, CA 92093-0218, USA. e-mail: mroughan@ucsd.edu

Abstract

Observations from an intensive oceanographic field program which took place in 1998-1999 about the separation point of the East Australian Current (EAC) show significant spatial and temporal variability of the EAC. Upstream of the separation point southward flowing currents are strong with sub-inertial velocities of up to 130 cms^{-1} in the near-surface waters, whereas downstream currents are highly variable in both strength ($1 - 70$ cms^{-1}) and direction. Upwelling is observed to occur through both wind-driven and current-driven processes, with wind effects playing a lesser role. By contrast, the encroachment of the EAC upon the coast has a profound effect on the coastal waters, accelerating the southward (alongshore) currents and decreasing the temperature in the bottom boundary layer (BBL) by up to 5°C. As the axis of the jet moves onshore negative vorticity increases in association with an increase in non-linear acceleration. During this time bottom friction is increased, the Burger number is reduced and the BBL shut-down time lengthens. The observed upwelling is attributed to enhanced onshore Ekman pumping through the BBL resulting from increased bottom stress as the southerly flow accelerates when the EAC encroaches across the continental shelf.

1 Introduction

Typically the surface waters of the East Australian Current (EAC) are low in nutrient concentrations, however in the vicinity of the EAC separation point, increased nutrient concentrations have been observed (Rochford, 1972, 1975). Rochford (1975) observed that the proximity of the EAC to the coast coincided with periods of nutrient uplift. From a series of satellite images of sea surface temperature (SST) combined with hydrographic (CTD) and velocity (ADCP) transects, Roughan and Middleton (2002) showed that when the core of the EAC moves closer to the coast, the isotherms are uplifted and nutrients are brought to the surface resulting in a phytoplankton bloom. Many hypotheses exist as to why upwelling occurs in the coastal region near where the EAC separates, for example Boland and Church (1981) and Blackburn and Cresswell (1993) cite a rapid flowing EAC near the continental shelf break whilst Tranter et al. (1986) suggests that the separation of the EAC from the coast plays a role in driving upwelling. More recently Oke and Middleton (2000) demonstrated through numerical simulations that topographic acceleration of the EAC plays a role in driving upwelling. In addition, a modelling study by Roughan et al. (2003) showed the importance of bottom friction on the continental shelf in the region.

Generally the EAC separates from the central eastern coast of Australia between $30 - 33°$S forming a sharp front in velocity and temperature as it turns eastward, where velocities of up to 2 ms^{-1} and a temperature front of up to 7°C have been observed (Godfrey et al., 1980; Boland and Church, 1981; Church and Freeland, 1987; Church and Craig, 1998, *inter alia*). The primary aim of this study is to examine the effects of the EAC on the coastal waters, in particular to investigate the question of current-driven upwelling and to identify the role of the EAC in driving cold nutrient laden water into the coastal region south of Smoky Cape (30°55′S).

The EAC is analogous to the Gulf Stream in that it is a warm intense western boundary current (WBC), however in contrast to the Gulf stream, in the region where the EAC separates from the coast, the continental shelf is very narrow (< 20 km). This proximity of the southerly EAC jet to the coast is conducive to uplifting of the isotherms across the narrow continental shelf which 'pre-conditions' the coastal waters such that they are upwelling favourable (Gibbs et al., 1998). Such pre-conditioning occurs to a far lesser extent in other WBCs as generally the shelf widths are much greater, insulating the coastal waters from the offshore currents.

Topography and bottom bathymetry influence flow across the continental shelf, particularly in the near shore region. This is true for tidal and wind induced currents, or coastally-trapped waves that propagate along the coast. In recent times transport through the bottom boundary layer (BBL) has been recognised to play a role in cross-shelf exchange. Theoretical studies by MacCready and Rhines (1991, 1993) and Garrett et al. (1993) investigated the Ekman transport through the bottom boundary layer and the shut-down of such flow (which may or may not occur) dependent on bottom slope. Lee et al. (2001) noted that in a strong WBC, bottom stress (τ_b) is influential to at least a depth of 300 m. Thus the concept of upwelling through the bottom boundary layer driven

by a strong western boundary current is of significance.

In order to elucidate the role of the EAC in current-driven upwelling an intensive oceanographic field experiment was conducted in the vicinity of the EAC separation point south of Smoky Cape (30°55′S), which is described in Section 2. This is followed in Section 3 by an investigation of the spatial and temporal variability observed in the temperature and current fields both upstream and downstream of the EAC separation point. Salient features of sub-inertial frequency fluctuations of current, and temperature observed upstream and downstream of the EAC separation are interpreted in both the horizontal and vertical. We examine time series of current velocity and temperature with emphasis on two upwelling events that occurred. During these events significant decreases in bottom temperature occurred however the mechanisms driving these two events are different. The first event is attributed to local wind forcing, whereas the second appears to be related solely to the encroachment of the EAC upon the coast. A detailed analysis of the current-driven event is presented in Section 4 including an examination of the dynamics in the BBL and estimates of BBL shut-down timescales for the region. Finally the findings are summarised in Section 5.

1.1 Current-Driven Upwelling

Onshore flow in the bottom boundary layer can occur as a response to interior flow along the continental shelf (poleward along an eastern coast in the southern hemisphere). Such Ekman transport acts to carry dense water up the slope, which can result in upwelling. In the flat bottom case across-shelf mass transport in the bottom boundary layer (M_x), can be approximated by $M_x = -\frac{1}{2}\rho v_g \delta$, (directed negative (positive), onshore (offshore)) where v_g is the average alongshelf geostrophic velocity (directed negative poleward), ρ is the density of the water and δ is the boundary layer thickness.

A schematic representation of current-driven upwelling is shown in Figure 1 where mass transport (M_x) through the BBL of thickness δ is shown as a response to the strong alongshore geostrophic current v_g which results in the uplift of water at a velocity w_c:

$$w_c = \frac{\frac{1}{2} v_g \delta}{R_{oi}} \tag{1}$$

with a length scale defined as the internal Rossby radius R_{oi}. In shallow water over a sloping bottom however buoyancy effects must be considered. Trowbridge and Lentz (1991) and MacCready and Rhines (1993) investigated the theoretical aspects of such flow over a sloping bottom and found that the resultant buoyancy force in the BBL opposed further Ekman flux causing the transport to decay and hence acted to 'shut-down' the Ekman transport though the BBL. The timescale (t) of this shut-down is proportional to $f/(N\alpha)^2$, where N is the buoyancy frequency, and α is the bottom slope. This can be expressed as $t = S^{-1} f^{-1}$ where $S \equiv N^2\alpha^2/f^2$ is the slope Burger number. Garrett et al. (1993) found that this tended to underestimate shut-down times, and determined a timescale of BBL arrest to be $(C_d N/f)^{-1/2} S^{-1} f^{-1}$ where N is the buoyancy frequency in the interior and C_d is a quadratic bottom friction coefficient. Ramsden (1995) cites

typical values of S for oceanographic regimes to be of order unity or less, where $N = O(3 \times 10^{-3})$ s^{-1},$f = O(10^{-4})$ s^{-1}, $\alpha = O(0.01 - 0.1)$.

1.2 Wind-Driven Upwelling

In the classical wind-driven upwelling model water in the surface layer is driven offshore by the alongshore component of the wind-stress (τ^y) and water upwells near the coast to replace the offshore directed Ekman transport (Smith, 1981) with an offshore scale given by the internal Rossby radius R_{oi} (Figure 1). Calculations of R_{oi} for our study region give values of $5 - 8$ km. The resultant across-shore Ekman volume transport (V) per unit length alongshore, is $V = \tau^y/\rho f$ and is confined to the surface Ekman layer (H_e) where ρ is the mean density of the surface mixed layer. The across-shore velocity (u_e) (depth averaged throughout the Ekman layer, H_e) attributed to an alongshore wind-stress (τ^y) can thus be given by $u_e = \tau^y/(\rho H_e f) = V/H_e$. The average vertical upwelling velocity (w) can be approximated by:

$$w = \frac{\tau^y}{\rho f R_{oi}} \tag{2}$$

The observations presented in following sections enable the investigation of wind-driven and current-driven upwelling on the east coast of Australia and a comparison of the effectiveness of the wind and the alongshore current in bringing nutrients to the surface.

2 Experimental Program

The study site extends along the coast of central eastern Australia from Urunga (30°S) to Port Stephens (33°S), and offshore from the coast to the 500 m isobath (Figure 2). This region spans the widely recognised location of EAC separation, as well as Smoky Cape, the narrowest point (16 km) of the continental shelf, (where the continental shelf is defined as the region extending seaward of the coast to the 200 m isobath).

2.1 The Mooring Arrays

The mooring program involved the deployment of two cross-shelf mooring arrays over a three month period from November 1998 − January 1999. One array was deployed at Smoky Cape, where the shelf is 16 km wide, the other array was deployed 90 km south of this point, directly offshore from Diamond Head (31°44′S) where the shelf widens to 30 km. The mooring arrays, which were designed to examine the three dimensional nature of the East Australian Current, are shown in Figure 2. Fourteen current meters (a mixture of 2D and 3D Falmouth Scientific Instruments (FSIs), Inter Ocean S4s and Aanderra RCM4s) were deployed in two mooring arrays positioned shore-normal across the continental shelf.

Optic Stowaway and Titbit temperature sensors were interspersed amongst the current meters throughout both arrays. The sampling interval was set to 3 minute averages over a 15 minute period for the FSIs, S4s and Titbits, and over a 30 minute period for

the Aanderras and Optic Stowaways. The Smoky Cape (SC) array (30°55′S), consisted of 3 moorings, Smoky Cape A (SCA), Smoky Cape B (SCB) and Smoky Cape C (SCC), spaced evenly across the continental shelf, deployed in 50 m, 100 m, and 150 m of water respectively. The Diamond Head (DH) array (31°44′S) consisted of four moorings, Diamond Head AA (DHAA), Diamond Head A (DHA), Diamond Head B (DHB), and Diamond Head C (DHC), deployed in 30 m, 50 m, 95 m, and 150 m water respectively. The Mooring Design and Dynamics program for Matlab (Dewey, 2000) was used to design the current meter moorings and estimate the mooring layover.

2.2 The Wind Stress Field

Typically local winds along the central eastern Australian coast are highly variable in strength and direction and upwelling favourable (northerly/poleward flowing) winds are rarely present for any duration, which is reflected in the observations presented here. Wind velocity measurements were obtained from a land-based weather station at Smoky Cape Light house, (31°54′S, 152°30′E) and were adjusted to a standard height of 10 m above sea level using a neutral stability wind profile. Comparisons between the land based weather and maritime winds obtained shipboard during the hydrographic surveys offshore from Smoky Cape showed that whilst the wind direction is represented accurately, coastal wind records tend to slightly underestimate the magnitude of those experienced at sea (Roughan and Middleton, 2002).

Table 1 gives the mean ($\bar{x}$) and standard deviation (σ) of the wind speed, direction and the alongshore (τ_y) and across-shore (τ_x) components of wind stress (Large and Pond, 1981). It is evident that the standard deviations are large when compared to the mean values, for example in the case of τ_x and τ_y, $\bar{x} = (-0.001, -0.002)$, and $\sigma = (0.007, 0.023)$ respectively. Furthermore the mean summer wind velocity ($3\ \mathrm{ms}^{-1}, 156°$) is not upwelling favourable.

3 Variability about the EAC Separation Point

The time series of sub-inertial velocities obtained are shown decomposed into the alongshore (Figure 3) and across-shore directions (Figure 4), where the top panel in both figures shows the alongshore wind-stress (τ_y). The co-ordinate system is orientated such that x is shore-normal positive offshore and y is alongshore positive equatorward with corresponding velocities $\mathbf{u}$=(u,v). The direction convention is such that positive wind-stress corresponds to equatorward wind forcing. The mean and standard deviations for each current velocity time series are presented in Table 2. These results reveal the variability of the currents about the EAC separation point.

At Smoky Cape the magnitude of the predominantly southward current decreases with depth through the water column, but increases eastward towards the core of the jet, with sub-inertial speeds up to 130 cms^{-1} in the near-surface waters. The current is strongly polarized in the alongshore direction and the alongshore component is highly correlated

vertically through the water column.

Upstream of the separation point both the mean and standard deviation in the along and across-shore directions are comparable in magnitude. The maximum mean flow of 77 cms^{-1} southward occurs at SCB_{20} (where the subscript denotes water depth), which decreases with depth to 48 cms^{-1} southward at SCB_{50} (Table 2). At SCA and SCB the mean speed of the mid-depth current is 60% of the near-surface current. The mean alongshore flow at Smoky Cape is aligned with the isobaths to within 5° and decreases in strength with depth. The only exception to this is at the mid-shelf mooring, where the near-surface waters are directed slightly more onshore.

The currents measured along the Diamond Head transect are more variable, weaker in strength, and less consistent in direction than those upstream at Smoky Cape. Inshore at Diamond Head (DHAA) the standard deviation of the across-shore flow (3.3 cms^{-1}) is more than an order of magnitude larger than the mean current (-0.1 cms^{-1}). In the alongshore direction the standard deviation of the inshore flow (7.9 cms^{-1}) is large compared to the mean current (0.9 cms^{-1}). At the offshore mooring (DHC), the standard deviation of the alongshore flow (29 cms^{-1}) is the same order of magnitude as the mean current (23.3 cms^{-1}). The mean current over the inner shelf (DHAA and DHA) is variable in strength and sheared in direction, and is generally small in magnitude and often directed equatorward, representative of the more complex fluctuations inshore of the southerly jet. The maximum mean flow (25 cms^{-1} southward) is in the near-surface waters mid-shelf, but it is 60% weaker than the mean current measured along the same isobath 90 km to the north. These results are consistent with satellite images which show that Smoky Cape is directly influenced by the warm EAC waters, whereas generally the coastal waters at Diamond Head are not.

The temporal variability of the EAC and its influence on the coastal currents suggests the partitioning of the time series into five specific events each of which is delineated by different salient features. The events are summarised as follows: *EAC 1*: 21 November 1998 − 7 December 1999, *Wind event*: 7 December 1998 − 15 December 1998, *Reversal event*: 25 December 1998 − 2 January 1999, *Current event*: 2 January 1999 − 13 January 1999, *EAC 2*: 13 January 1999 − 24 January 1999. Each of these events are marked on Figures 3−5 by 'E1, W, R, C, and E2' respectively.

The *Reversal event* is noted for the sudden and strong reversals in the current speed and direction. At the onset of this event the EAC flows strongly southward with speeds of up to 1 ms^{-1} recorded at the Smoky Cape moorings. During the event the current oscillates between stronger northward and weaker southward flow.

The temporal means of the alongshore currents are small and the standard deviations are high, indicating that alongshore oscillations dominate the event. The mean near-surface currents at Smoky Cape are < 20 cms^{-1} southward, which is nearly an order of magnitude smaller than the maximum current strength measured. In many instances the standard deviations in both the along and across-shore directions are more than double the mean flow. During this event the current regime shifts from being a strong baroclinic southerly flowing jet to oscillating alongshore in a near barotropic manner. During this time, changes in the current direction occur with a period of ~ 3 days and the near-surface

currents at Smoky Cape are highly coherent with fluctuations in sea level elevation at Port Macquarie (31°25′S 152°54′E), which is consistent with the propagation of coastally trapped waves throughout the region (Roughan, 2002).

There are two periods where the EAC is flowing swiftly southward adjacent to the coast between Smoky Cape and Diamond Head. These events are referred to as *EAC 1* and *EAC 2* and are marked on the figures as E1 and E2. During these two events the currents are strongly southward, with velocities of more than 1 ms^{-1} at SCB and SCC. Surface velocities are strongest at Smoky Cape during *EAC 1* and *EAC 2*. Inshore at SCA_{15} the mean velocities $(\bar{u}, \bar{v})$ are slightly weaker during *EAC 1* ($\bar{v} = -67$ cms^{-1}) than *EAC 2*, ($\bar{v} = -80$ cms^{-1}), however offshore and at depth (SCC), the velocities are 20% stronger during *EAC 1*, ($\bar{v} = -101$ cms^{-1}) than during *EAC 2* ($\bar{v} = -76$ cms^{-1}).

At Diamond Head the maximum mean velocities occur during *EAC 2* when the core of the current is located well onshore indicating that the EAC has encroached upon the shelf. At both arrays the currents have a slight cross-isobath flow, directed onshore at Smoky Cape, where the near-surface velocities are up to 25 cms^{-1}. This is an order of magnitude larger than the onshore currents during any other event. Downstream of the separation point the cross-shelf flow is directed seaward at the two outer moorings. For the remainder of the experiment the EAC separated from the coast between Smoky Cape and Diamond Head.

During the *Wind event* velocities are strong and southward at Smoky Cape ($\bar{v} = -67$ cms^{-1} and $\bar{v} = -75$ cms^{-1} at SCA_{15} and SCB_{20} respectively) and weak and fluctuating at Diamond Head ($\bar{v} = 5$ cms^{-1}, $\sigma = 12$ cms^{-1} and $\bar{v} = -25$ cms^{-1}, $\sigma = 27$ cms^{-1} at DHA_{35} and DHB_{20} respectively). Towards the end of the event the currents accelerate to a maximum of 1 ms^{-1} at SCB_{20} and ~ 0.5 ms^{-1} at DHB_{20} where the peak velocity coincides with the maximum wind strength on December 12 (Figure 3) aided by an encroachment of the jet. After this time both the wind and the alongshore jet relax.

The *Current event* is distinguished by a strengthening of the southward velocity across both mooring arrays as the flow encroaches upon the shelf. Initially mid-shelf (SCB) the flow is northwards at speeds of up to 0.5 ms^{-1}, however by 15 January the flow is again southward with a mean speed of 1 ms^{-1} in the near-surface waters at SCB. At Smoky Cape the across-shore flow changes from offshore or almost negligible to onshore with a speed of up to 40 cms^{-1} in the near-surface waters.

Twenty-six HDL temperature loggers were distributed throughout the water column across the two mooring arrays as indicated by the $\times$ in Figure 2. Temperature was also measured by the 6 FSI current meters. The raw temperature time series were low-pass filtered using a Lanczos-cosine filter with a cut off period of 36 h and are shown in Figure 5. There is an obvious warming trend which occurs throughout the period which spans the Austral summer and the water is noticeably stratified. There is a vertical temperature change of $4 - 5$°C at DHA and SCA, and over the 100 m isobath the vertical change in temperature is $6 - 7$°C at DHB and SCB.

The temperature time series reveal two periods where there is a decrease in bottom temperature of up to 5°C across both mooring arrays. The first occurs from $7 - 15$ December 1998 (hereafter referred to as the *Wind event*) and the second occurs from $2 - 11$

January 1999 (the *Current event*). During the *Wind event*, strong northerly (upwelling favourable) winds are present, followed by a 5°C decrease in the bottom temperature across both mooring arrays over a 5 day period.

The *Current event* is characterized by a rapid drop in bottom temperature across both mooring arrays that is seemingly unrelated to local winds. The bottom temperature across the Smoky Cape array decreases more than 5°C throughout the period, whilst the surface temperature shows little change (Figure 5). At Diamond Head the temperature decrease is seen initially in the bottom boundary layer, but by 9 January even the surface waters at DHA and DHB are considerably colder than at the start of the event. Figure 5 shows that from $1-8$ January the alongshore wind stress is weak, building to a peak around 9 January. This peak however was a maximum of 0.06 Pa, and of less than 24 h duration which is insufficient to drive such a substantial upwelling.

The mean temperatures at each thermistor are shown in Figure 6 as a function of depth, also shown are the mean temperatures during the wind and current events. At Diamond Head the mean surface temperature increases 2°C offshore with increasing proximity to the EAC, this is in contrast to the surface waters at SC where the temperature remains steady moving offshore. As expected, temperature decreases with depth at both arrays. Inshore, surface temperatures at Diamond Head are consistently colder than those 90 km to the north at Smoky Cape. On average the water at SCB is 3°C warmer at depths of 20 and 50 m than at DHB to the south. At a depth of 88 m mid-shelf and at the shelf break mooring the mean temperature to the north (SCC) is consistently 1°C warmer than that at DHC. This suggests that for a large part of the experiment period the EAC does not directly influence the coastal waters at Diamond Head.

The time series show two significant decreases in bottom temperature, the first being during the *Wind event* and the second during the *Current event*. The mean temperatures in the BBL are consistently $2-3$°C colder during the *Current event* than those measured at any other time. Upstream of the separation point, although the bottom temperatures are cooler during the *Current event* than the *Wind event*, the mean surface temperatures are warmer. At SCA there is a mean vertical temperature change of 8°C over 50 m during the *Current event*. At DHAA inshore of the EAC jet the surface waters are cooler by $2-3$°C throughout the water-column during the *Current event*. These results indicate a warming of the surface waters and a cooling of the bottom waters as the EAC moves onshore, suggesting that the encroachment of the current drives upwelling at depth.

4 Encroachment of the EAC and Upwelling

Here we identify the temperature response to the encroachment of the current upon the shelf as current-driven upwelling. As the current encroaches upon the coast it can act to accelerate the alongshore current which causes uplift of the isotherms as the entire axis of the current moves onshore as a jet. This is readily distinguishable from onshore advection as a response to downwelling favourable winds which causes homogenisation and depression of the isotherms and can act to relax or even reverse the flow.

A schematic representation of upwelling as a response to the encroachment of the EAC (Figure 7) shows a strong alongshore jet with the core centered seaward of the shelf break. The sloping lines represent the isotachs of the jet. As the core of the current encroaches upon the continental shelf the isotachs are uplifted. The increase in strength of the current at the base of the water column causes an increase in bottom friction and if the strength of the current is sufficient, enhanced Ekman pumping will occur through the BBL which in the Southern Hemisphere is directed onshore ($f < 0$), thus the isotherms are uplifted and upwelling occurs.

4.1 The Current Event

Satellite images have shown that the proximity of the core of the EAC to the coast fluctuates in the Smoky Cape region, evident in the velocity time series presented in Figures 3 and 4. Associated with these fluctuations in proximity are changes in the strength of the current and the temperature of the shelf waters. The satellite images of SST in Figure 8 clearly show the core of the EAC moving closer to the coast over a 10 day period. The image from 27 December 1998 (Figure 8a) shows a warm jet flowing southward adjacent to the continental shelf to about 31°S where the current separates from the coast between Smoky Cape and Diamond Head. After separation the jet flows directly southward virtually along the 153°E parallel for 150 km, where upon it turns 90° and heads eastward, before meandering southward again with the main jet more than 300 km from the coast.

The SST image from 7 January 1999 (Figure 8b) shows that the EAC separation point has moved further to the south indicating an encroachment of the current. The eastward bend is less pronounced, and the turning point has been advected more than 150 km to the south. Locally at Diamond Head this current encroachment has the effect of stronger velocities which are evident in the velocity fields in Figures 3 and 4. The SST image (Figure 8b) shows colder water hugging the coast at Diamond Head and in the vicinity of Port Stephens.

Figure 9 shows the time series of the alongshore wind-stress (τ^y), the alongshore depth-averaged currents at SCA, SCB, and DHB, and the surface and bottom temperature at SCA, SCB and DHAA, during the *Current event* (Figure 9 b-d). Throughout this time the alongshore wind-stress (τ^y) is weak (Figure 9 a) until it increases for ~ 36 h starting on January 7, and peaking with a maximum alongshore (upwelling favourable) wind-stress of ~ 0.06 Pa on January 8. This event occurs more than 6 days *after* the temperature decrease begins in the BBL at SCA (Figure 9 b).

The dependent relationship between alongshore current and temperature in the BBL is evident across the narrow shelf. From 26 December to 2 January the barotropic alongshore current fluctuates with a period of $2-3$ days. Coincident with this is a 1°C temperature change which lags the current by half a day in the BBL. By 2 January 1999 the current reverses strongly for the final time turning southward and the temperature begins to decrease, lagging the current by 24 h in the BBL. As the current continues to accelerate the temperature decrease continues.

Mid-shelf at Smoky Cape, the near-surface current changes direction from a northward flow of 0.25 ms^{-1} to a southward flow of more than 1 ms^{-1} in the space of 9 days. In this time the temperature in the BBL drops 4°C and the barotropic current increases to $\sim$ 60 cms^{-1}. Figure 5 shows an increase in temperature mid-water and in the surface as the axis of the jet moves onshore, particularly at SCC and DHC. At Diamond Head (Figure 9 d) the cold water is upwelled all the way to the surface, This possibly indicates an uplifting of water at Smoky Cape and a downstream advection of colder water which is eventually upwelled to the surface at Diamond Head. As the core of the current moves onshore the current over the continental shelf accelerates particularly at SC and colder water is driven onshore through the BBL reaching the surface to the south at DH on the coastal side of the temperature front.

After $\sim$ 8 days the current ceases accelerating and finally weakens by 30 cms^{-1} in the near-surface waters at SCA and SCB, and actually reverses at DHB (Figure 9 d). Following this weakening the temperature in the BBL increases again, presumably as the mass transport through the BBL decreases and the flow relaxes down the slope. Furthermore as the EAC flow once again becomes steady the BBL begins to shut-down once again.

4.2 EAC Acceleration

The relative depth averaged vorticity at any location is given by: $\zeta = \partial\bar{v}/\partial x - \partial\bar{u}/\partial y$. The time series of the depth averaged vorticity is calculated at SC where $\partial\bar{v}/\partial x$ is estimated across the mooring array and estimates of $\partial\bar{u}/\partial y$ are small by scaling arguments. During the *Current event* the EAC flow accelerates (Figure 10 b) as it encroaches upon the coast and the bottom temperature decreases (Figure 10 c). Co-incident with this is a temporal increase in relative vorticity at Smoky Cape indicating shear in the depth averaged flow. When the EAC flow accelerates during the *Current event* ζ becomes more negative (Figure 10 d) immediately preceding the decrease in temperature in the BBL at both Smoky Cape and Diamond Head. This coincides with higher Rossby number which indicates a non-linear (advective) acceleration of the flow over the shelf proper.

Figure 10 e shows the time series of bottom stress (τ_b) at DHB where $\tau_b = \rho r v_g$ with a linear drag coefficient, $r = 5 \times 10^{-4}$ ms^{-1} (Lentz and Winant, 1986) and v_g is the barotropic alongshore velocity at DHB. The small value of r is appropriate as the velocity is from outside the BBL. Qualitatively the estimates of τ_b show that the increase in bottom stress coincides with the increase in non-linear acceleration of the flow, and the decrease in temperature in the BBL.

4.3 The Bottom Boundary Layer

Numerical simulations by Oke and Middleton (2000) indicate that alongshore topographic variations can impact on shelf circulation by accelerating the alongshore flow through a narrowing shelf cross section. Smoky Cape is the narrowest point on the eastern Australian continental shelf (16 km) narrowing from twice that width a distance of 50 km to the

north. Investigations of the dynamics in an idealised simulation of the region showed that an acceleration of the flow caused an increase in bottom stress which in turn decreases the gradient Richardson number Ri, thus enhancing vertical mixing. The slope Burger number (S) is reduced hence the time it takes for the BBL to shut-down is lengthened. Thus deeper waters can be transported up the slope through the BBL for an extended period of time which can result in upwelling. The observations presented here show the presence of upwelling driven by the EAC in the Smoky Cape region where the continental shelf narrows.

To investigate the relationship between stratification, bottom slope and temperature in the BBL the time series of S is calculated from the observations across the continental shelf at both Smoky Cape and Diamond Head. The interior buoyancy frequency (N) is obtained from measurements of temperature and salinity during repeat hydrographic stations during November 1998 and January 1999. At other times N is calculated from temperature and regressions of salinity which are compared with the climatology in the region. Figure 11 shows time series of alongshore velocity (v) at SCB and DHB (Figure 11 a,b), temperature (T) at DHB and Burger number (S) at both DHA and DHB (Figure 11 d).

At DHA, S decreases from 26 December - 8 January as the axis of the EAC moves onshore and the flow is accelerated to the north at Smoky Cape (Figure 11 a). The lower Burger number ($S \sim 0.1$) indicates that it is possible for the bottom boundary layer to remain active for a longer period of time, thus allowing prolonged upwelling to occur. The temperature decreases $3 - 4$°C indicating upwelling during these two periods. After this time S increases again as the EAC dominates the coastal circulation at DH, and bottom temperatures increase again.

Throughout the time S ranges $0.01 - 2$ at DH and tends to remain lower than at SC, which is related to less stratification and a more gentle bottom slope ($\alpha = 3.9 \times 10^{-3}$ at DHB and $\alpha = 7.5 \times 10^{-3}$ at SCB). S is far more variable at DH, dictated by the frequent mixing and reduced stratification. Mid-shelf at DH, bottom slope is much reduced from that at the other moorings, and it is here that shut-down time scales are longest ($S < 0.5$).

Lentz and Trowbridge (1991) found that the bottom mixed layer height is dependent on the strength and direction of the overlying current as well as the interior stratification. Furthermore there is an asymmetric response to poleward and equatorward currents, where the BBL is thicker in downwelling favourable flows than in upwelling favourable flows. In this region the current is predominantly upwelling favourable, however the thickness of the BBL (and hence the near bottom vertical temperature stratification) does change with time (Figure 5). Across the shelf at Diamond Head the vertical temperature gradient reduces to a minimum during the *Current event* when the currents increase in strength and upwelling occurs, during which time the BBL increases to at least 15 m thick at DHA and DHB.

4.4 Shut-down Timescales

In their analysis of flow through the bottom boundary layer Trowbridge and Lentz (1991) and MacCready and Rhines (1991) both assumed flat interior isopycnals, combined with a steady along-slope velocity outside the boundary layer. Clearly in this case the flow is not steady and the isopycnals are not flat. Gibbs et al. (1998) showed that the uplifted isopycnals to the west of the core of the EAC contributed to 'pre-conditioning' of the continental shelf waters which favored wind-driven upwelling. Furthermore in this region the accelerated flow around Smoky Cape will act to increase the pressure gradient through an increase in centripetal acceleration which will result in further uplift of the isopycnals.

Such shut-down theory was developed for an idealised situation with flat isopycnals intersecting the slope, hence it is not simple to apply it to the three-dimensional ocean environment. Shut-down estimates obtained for our study site vary greatly depending on the stratification and the method used. At SCA where $\alpha = 7.5 \times 10^{-3}$ and $f = -7.491 \times 10^{-5}\mathrm{s}^{-1}$, the parameters $N = 0.01$ s^{-1} and $S \approx 1$ give arrest times ranging from 3 h (MacCready and Rhines, 1993) to 7 h (Garrett et al., 1993). In contrast, at DHB where the bottom slope is half that at SCB and the stratification is reduced, arrest times are longer. For example, from $2-6$ January during the *Current event* ($\alpha = 3.9 \times 10^{-3}$, $f = -7.669 \times 10^{-5}\mathrm{s}^{-1}$) the arrest time at DH is $3-8$ days when $S \approx 0.05 - 0.1$ using the method of Garrett et al. (1993). This emphasizes the importance of α the bottom slope, where a gentle slope allows for greater mixing and hence a reduction in N which in turn allows for a longer shut-down timescale. When the flow is non-steady the increase in bottom stress enhances flow through the BBL thus driving colder water into the surface waters at the coast. As the current moves onshore at Smoky Cape, the isotherms are uplifted, bottom friction increases and the bottom temperature decreases at both Smoky Cape and Diamond Head. At Diamond Head the colder, nutrient rich water is actually uplifted all the way to the surface, resulting in upwelling.

Sensitivity experiments by Oke and Middleton (2001) showed that the magnitude of topographically-driven upwelling resulting from the narrowing of the continental shelf is dependent on the strength of the current. Furthermore, it was shown that when the slope of the uplifted isopycnal matches the bottom slope, along isopycnal mixing is optimised, thus allowing slope water to be upwelled to the surface without the opposing effects of buoyancy. This implies that nutrient enrichment of the coastal waters will also be enhanced under these conditions. The results of Roughan and Middleton (2002) show that as the current weakens at Smoky Cape, horizontal stratification returns and nutrient supply ceases as does the biological response.

5 Discussion

The currents in the Smoky Cape region are highly variable, in both strength and direction, and these variations dominate the coastal environment having a profound effect on the temperature structure of the coastal and shelf waters. The time series presented here show that a significant decrease in bottom temperature occurs concurrently with the

encroachment of the EAC upon the continental shelf. It appears that current-driven upwelling is occurring as a response to an increase in the non-linear acceleration of the flow.

Furthermore a more gentle bottom slope and an increase in mixing at DH results in a low Burger number, thus making it more conducive to Ekman pumping through the bottom boundary layer. During the current encroachment event the temperature in the BBL decreases both at Smoky Cape and Diamond Head, however downstream at Diamond Head the shut-down time is lengthened such that the temperature decrease propagates into the surface waters. This suggests an uplift at Smoky Cape and southward advection, which results in upwelling to the surface downstream at Diamond Head.

Gibbs et al. (1998) found that wind-driven upwelling was more significant than upwelling driven by EAC eddy intrusions in the Sydney region after the EAC had separated from the coast. The observations presented here show the importance of current-driven upwelling in the vicinity of Smoky Cape when the EAC flows adjacent to the coast. Generally local winds are light and wind events of any significant length tend to be downwelling favourable. The ratio of the current-driven vertical uplift (Equation 1) to the wind-driven vertical uplift (Equation 2) is $\frac{1}{2}v_g\delta\rho f/\tau^y$. Substituting typical values of $\rho = 1000$ kg m^{-3}, and $\tau = 0.1$ Pa gives a ratio of $\sim 5 - 7.5 \times v_g$, depending on the thickness of the BBL (typically $10 - 15$ m in this region during upwelling). Hence it follows that on the SC shelf where coastal wind-stress is small ($\tau < 0.1$ Pa) and where swift alongshore currents flow adjacent to the coast ($v_g \sim 1$ ms^{-1}) current-driven upwelling can be substantially more effective than wind-driven upwelling in driving nutrient rich water to the surface by the coast. Furthermore the temperature response during the two events differs, with BBL temperatures $2 - 3$°C warmer during the *Wind event* than the *Current event*.

Roughan et al. (2003) investigated the importance of non-linearities in the EAC through a modelling study of the climatological currents in the Smoky Cape region. The findings show that upstream of the separation point the advective acceleration term $v.\partial v/\partial y$ is important as the current accelerates. Here observations show that the acceleration of the current at the shelf break results in a significant decrease in bottom temperature in the coastal waters locally and downstream. The EAC can be accelerated in the region either through encroachment of the current across the shelf, or through topographic acceleration where the continental shelf narrows at Smoky Cape. If the proximity and acceleration of the current is adequate, then bottom stress is increased and the bottom boundary layer shut-down time is lengthened. Hence Ekman pumping through the bottom boundary layer is prolonged and current-driven uplift occurs, resulting in upwelling further downstream.

6 Acknowledgements

The field program was conducted from the *R.V. Franklin* and the professional support provided by the ship's crew and the CSIRO personnel is gratefully acknowledged. The implementation of the field program depended on co-operation and assistance from a large

number of people all of whom deserve credit for its success, in particular Greg Nippard is thanked wholeheartedly for his dedication to the mooring program. We are grateful for the detailed comments from three anonymous reviewers. This work was supported by the Australian Research Council and CSIRO Marine Research supplied the SST images.

References

Blackburn, S. I., and G. Cresswell, 1993: A Coccolithophorid bloom in Jervis Bay, Australia. *Aust. J. Mar. Freshw. Res.*, **44**, 253–60.

Boland, F. M., and J. A. Church, 1981: The East Australian Current 1978. *Deep-Sea Res.*, **28**, 937–957.

Church, J. A., and P. D. Craig, 1998: Australia's shelfseas: Diversity and complexity. In Robinson, A. R., and K. H. Brink (Eds.), *The Sea*, Vol. 11, pp. 933–964. John Wiley & Sons, Inc., New York.

Church, J. A., and H. J. Freeland, 1987: The energy source for the coastal trapped waves in the Australian Coastal Experiment region. *J. Phys. Oceanogr.*, **17**, 289–300.

Dewey, R. K., 2000: Mooring design and dynamics - a matlab package for designing and analyzing oceanographic moorings. *Marine Models*, **1**, 103–157.

Garrett, C., P. MacCready, and P. Rhines, 1993: Boundary mixing and arrested Ekman layers: Rotating stratified flow near a sloping boundary. *Annu. Rev. Fluid. mech.*, **25**, 291–323.

Gibbs, M. T., J. H. Middleton, and P. Marchesiello, 1998: Baroclinic response of Sydney shelf waters to local wind and deep ocean forcing. *J. Phys. Oceanogr.*, **28(2)**, 178–190.

Godfrey, J. S., G. R. Cresswell, T. J. Golding, and A. F. Pierce, 1980: The separation of the East Australian Current. *J. Phys. Oceanogr.*, **10**, 430–440.

Large, W. S., and S. Pond, 1981: Open ocean momentum flux measurements in moderate to strong winds. *J. Phys. Oceanogr.*, **11**, 324–336.

Lee, S. K., J. L. Pelegri, and J. Kroll, 2001: Slope control in western boudary currents. *J. Phys. Oceanogr.*, **31**, 3349–3360.

Lentz, S. J., and J. H. Trowbridge, 1991: The bottom boundary layer over the northern California shelf. *J. Phys. Oceanogr.*, **21**, 1186–1201.

Lentz, S. J., and C. D. Winant, 1986: Subinertial currents on the Southern Californian Shelf. *J. Phys. Oceanogr.*, **16**, 1737–1750.

MacCready, P., and P. Rhines, 1991: Buoyant inhibition of Ekman transport on a slope and its effect on stratified spin-up. *J. Fluid. Mech.*, **223**, 631–661.

MacCready, P., and P. Rhines, 1993: Slippery bottom boundary layers on a slope. *J. Phys. Oceanogr.*, **23**, 5–22.

Oke, P. R., and J. H. Middleton, 2000: Topographically induced upwelling off Eastern Australia. *J. Phys. Oceanogr.*, **30**, 512–531.

Oke, P. R., and J. H. Middleton, 2001: Nutrient enrichment off Port Stephens: The role of the East Australian Current. *Cont. Shelf Res.*, **21**, 587–606.

Ramsden, D., 1995: Response of an oceanic bottom boundary layer on a slope to interior flow. Part 1: Time independent interior flow. *J Phys. Oceanogr.*, **25**, 1672–1687.

Rochford, D. J., 1972: Nutrient enrichment of East Australian coastal waters. 1. Evans Head upwelling. *CSIRO Aust. Div. Fish. Oceanogr. Rep.*, **33**.

Rochford, D. J., 1975: Nutrient enrichment of East Australian coastal waters. 2. Laurieton upwelling. *Aust. J. Mar. Freshw. Res.*, **26**, 233–43.

Roughan, M., and J. H. Middleton, 2002: A comparison of observed upwelling mechanisms off the east coast of Australia. *Cont. Shelf Res.*, **22(17)**, 2551–2572.

Roughan, M., P. R. Oke, and J. H. Middleton, 2003: A modelling study of the climatological current field and the trajectories of upwelled particles in the East Australian Current. *J. Phys. Oceanogr.*, **33(12)**, 2551–2564.

Roughan, M., 2002: *On the East Australian Current: Upwelling and Separation.* Ph.D. thesis, University of New South Wales, Sydney, Australia.

Smith, R. L., 1981: A comparison of the structure and variability of the flow field in three coastal upwelling regions: Oregon, North West Africa, and Peru. In Richards, F. A. (Ed.), *Coastal Upwelling*, Vol. 1 of *Coastal and Estuarine Sciences*, pp. 107–118. American Geophysical Union, Washington, D. C. 529 pp.

Tranter, D. J., D. J. Carpenter, and G. S. Leech, 1986: The coastal enrichment effect of the East Australian Current eddy field. *Deep-Sea Res.*, **33**, 1705–1735.

Trowbridge, J. H., and S. J. Lentz, 1991: Asymmetric behaviour of an oceanic boundary layer over a sloping bottom. *J. Phys. Oceanogr.*, **21**, 1171–1185.

List of Figures

List of Tables

	Speed (ms^{-1})	Direction ($^\circ$)	τ_x	τ_y
$\bar{x}$	3.0	156.3	-0.001	-0.002
σ	2.0	136.5	0.007	0.023

Table 1: Mean ($\bar{x}$), and standard deviation (σ) of raw wind speed and direction measurements and the lowpass filtered wind stress (Pa) in the across-shore (τ_x) and alongshore (τ_y) directions recorded at the land based weather station at Smoky Cape throughout the experimental period.

		Total		EAC 1		Wind		Reversal		Current		EAC 2	
		u	v	u	v	u	v	u	v	u	v	u	v
SCA_{15}	$\bar{x}$	−3.2	−54.1	−0.9	−66.9	−3.0	−66.7	−3.3	−14.6	−3.7	−41.8	−2.2	−79.4
	σ	4.3	29.1	3.0	12.6	4.8	20.9	4.5	31.2	4.2	30.6	4.6	14.2
SCA_{35}	$\bar{x}$	−1.1	−33.6	2.8	−46.2	−0.03	−43.9	−1.4	−4.0	−1.3	−22.1	−3.5	−56.2
	σ	3.3	25.2	2.5	12.6	2.6	16.0	2.4	24.6	2.0	20.6	2.8	11.1
SCB_{20}	$\bar{x}$	−20.6	−77.2	−25.8	−106.4	−16.4	−74.5	−13.4	−29.4	−10.2	−43.5	−24.3	−102.5
	σ	9.2	32.4	3.4	11.3	5.9	23.7	13.3	35.6	8.1	31.2	5.0	8.4
SCB_{50}	$\bar{x}$	0.5	−48.0	2.8	−71.5	−8.8	−55.7	−4.0	2.2	−2.6	−26.5	−20.9	−69.9
	σ	10.8	30.1	9.6	7.9	5.3	19.6	10.9	29.4	5.9	33.5	6.8	15.3
SCB_{80}	$\bar{x}$	−1.0	−28.4	−2.2	−53.2	−1.3	−42.8	−1.9	4.6	1.6	−11.0	0.9	−52.3
	σ	3.9	30.4	3.1	11.1	2.8	16.6	5.2	28.5	2.3	21.5	3.5	17.7
SCC_{80}	$\bar{x}$	−13.9	−56.0	−12.4	−100.9	−17.6	−56.1	−4.9	−4.8	−9.5	−18.4	−17.9	−77.0
	σ	7.1	35.6	3.1	16.8	3.2	26.5	9.0	25.6	8.4	23.4	3.5	11.3
$DHAA_{15}$	$\bar{x}$	−0.1	0.9	0.9	0.6	−2.1	0.4	−0.5	0.1	−0.3	−1.9	0.3	5.5
	σ	3.3	7.9	3.3	6.5	3.4	8.0	3.1	8.5	2.4	8.7	3.4	6.6
DHA_{20}	$\bar{x}$	−0.1	2.0	−0.2	5.8	−2.4	3.6	0.1	−0.9	5.5	−17.4	−1.3	5.0
	σ	6.0	16.3	5.2	10.5	5.8	16.5	5.6	14.1	9.6	17.8	4.9	15.7
DHA_{35}	$\bar{x}$	2.2	2.3	2.5	2.0	1.6	4.8	1.3	2.9	−1.5	−4.7	1.17	3.2
	σ	5.1	10.9	4.4	8.8	5.4	12.2	5.1	9.8	4.9	11.9	3.7	12.4
DHB_{20}	$\bar{x}$	3.5	−25.5	−2.1	−25.9	0.9	−25.0	2.6	−4.6	−8.8	−30.5	11.9	−66.6
	σ	11.7	28.7	7.7	19.5	8.7	26.9	7.6	19.7	8.2	23.9	12.4	7.7
DHB_{50}	$\bar{x}$	1.1	−9.3	0.1	−17.4	0.9	−15.5	−2.5	7.5	−2.7	−19.4	1.9	−30.0
	σ	5.4	22.8	6.2	14.0	3.7	19.2	4.4	14.4	4.4	21.5	3.0	18.0
DHC_{80}	$\bar{x}$	1.6	−23.3	4.5	−41.6	0.5	−14.7	−0.3	2.9	−1.2	−6.5	2.1	−68.5
	σ	3.6	29.1	3.9	21.7	1.1	5.2	3.5	10.3	2.4	10.3	4.0	21.1

Table 2: Mean ($\bar{x}$) and standard deviation (σ) of the alongshore (v) and across-shore (u) current velocities as measured by each current meter for the total time series and each of the 5 events at the SC and DH moorings. The numeral subscript indicates the depth of the instrument.

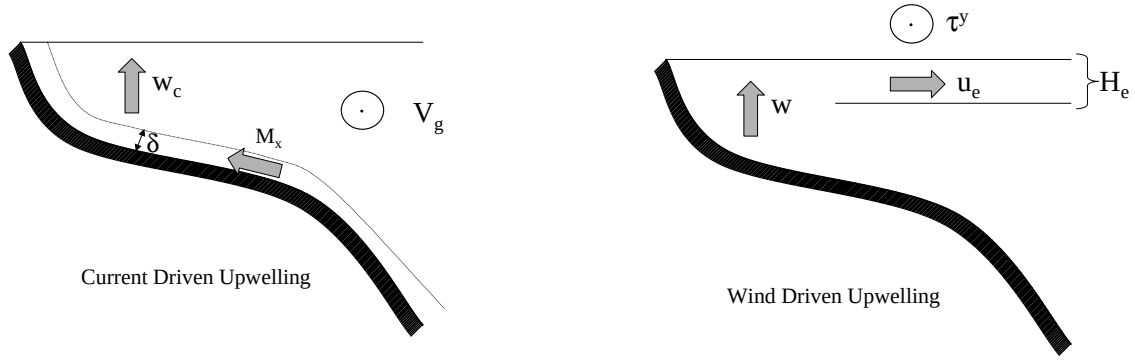

Figure 1: Left: Schematic representation of current-driven upwelling in the southern hemisphere. The average alongshore geostrophic current is v_g, M_x is the mass transport through the BBL of thickness δ and w_c is the current-driven uplift that occurs within R_{oi}. Right: Schematic representation of wind-driven upwelling. τ^y is the alongshore wind stress, u_e is the offshore velocity component in the Ekman layer of thickness H_e and w is the vertical wind-driven upwelling velocity.

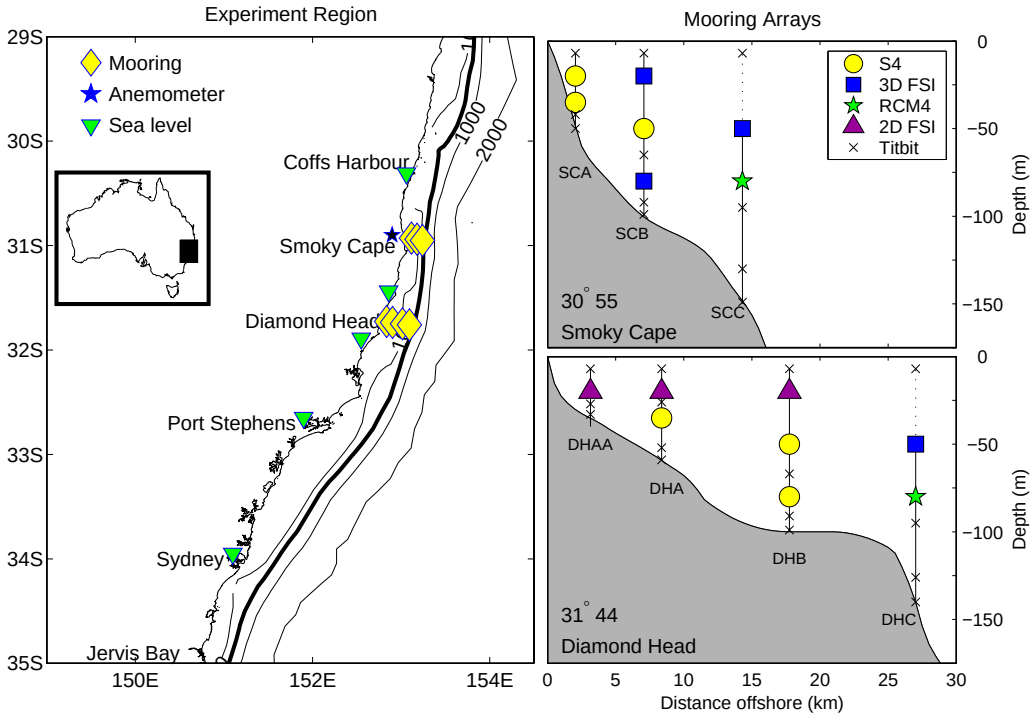

Figure 2: Left: The experiment region, in the vicinity of Smoky Cape, NSW, Australia. The locations of the moorings are denoted by $\diamondsuit$, sea level recorders by $\triangledown$ and anemometer location by $\star$. The 100, 200, 1000 and 2000 m isobaths are shown. The 200 m isobath is marked in bold. Distance scales are defined as follows: 1 ° of latitude = 60 nautical miles = 111 km. Right: Schematic diagram of the across-shore location of the mooring arrays (Upper: Smoky Cape, Lower: Diamond Head) showing the position and type of current meters and temperature sensors as described in the text. The dotted line indicates a snapped mooring.

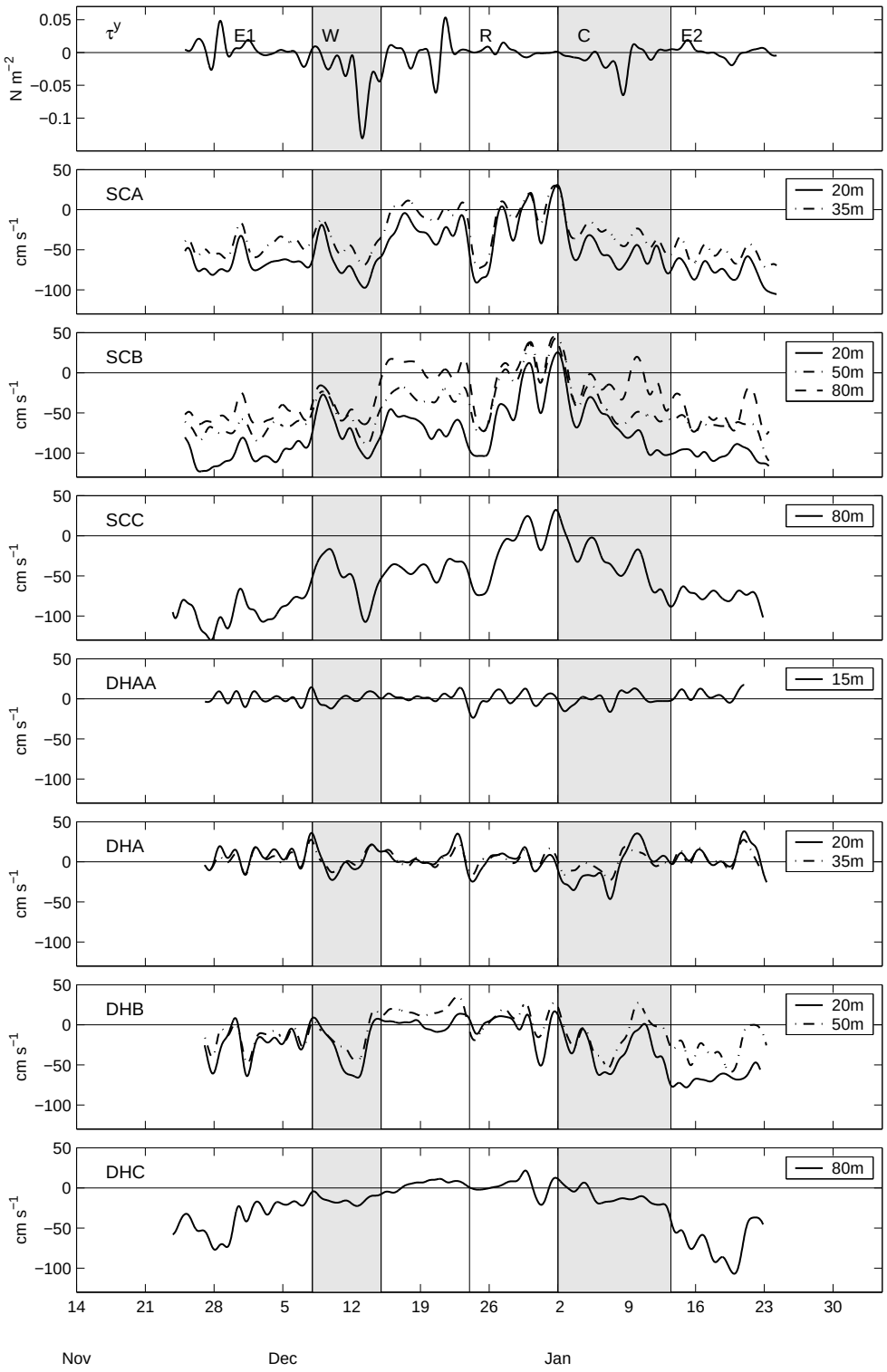

Figure 3: Time series of the alongshore wind stress and the sub-inertial alongshore current velocities at Smoky Cape and Diamond Head.

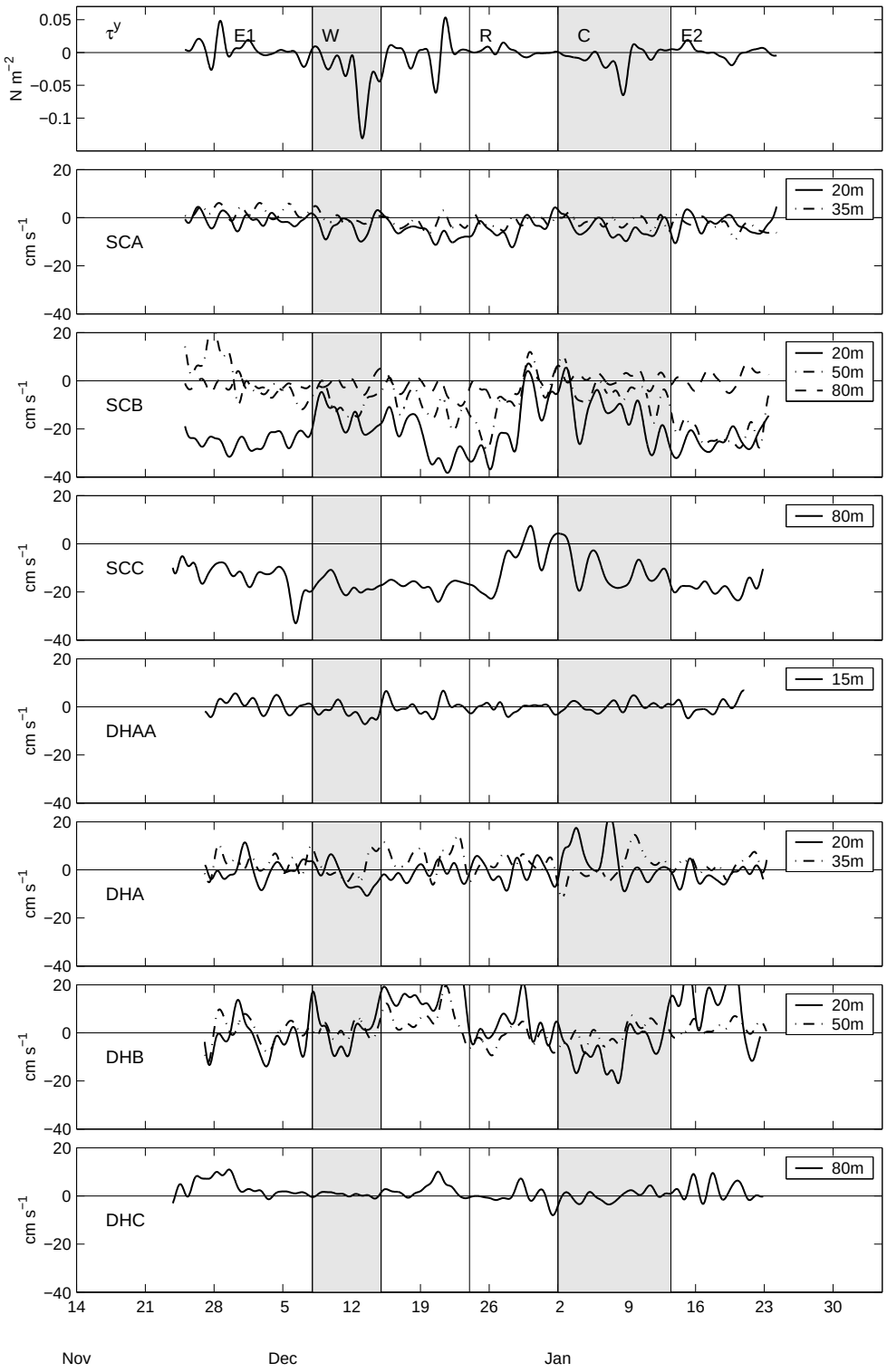

Figure 4: Time series of the alongshore wind stress and the sub-inertial across-shore current velocities at Smoky Cape and Diamond Head.

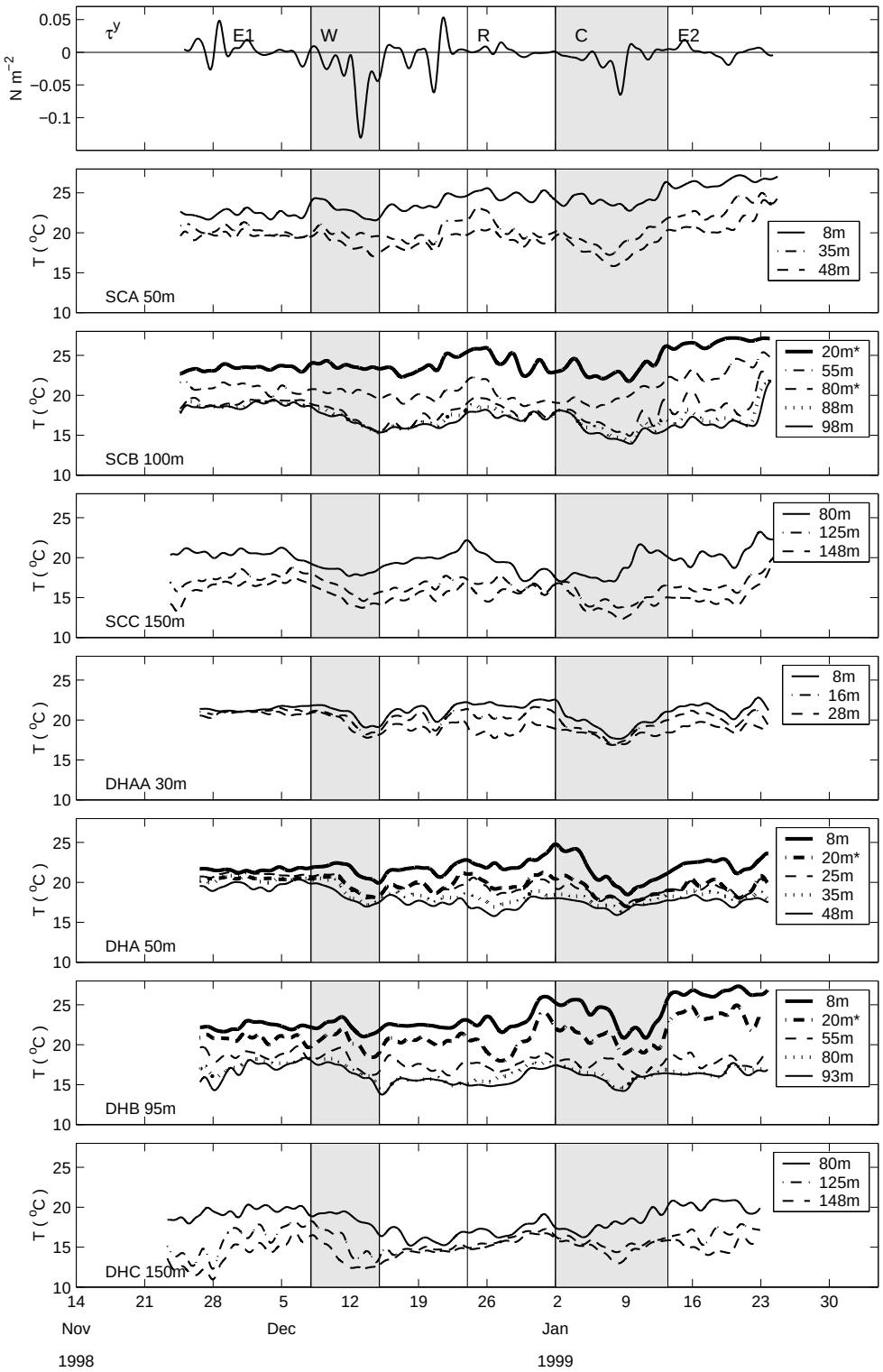

Figure 5: The top panel is the alongshore wind stress measured at Smoky Cape, the other panels show the temperature at Smoky Cape and Diamond Head which have been low-pass filtered with a cut off period of 36 hours. All records are measured with an HDL temperature sensor, except records measured concomitantly with current by FSI current meters (denoted by $*$). As in subsequent figures, each event is marked *EAC 1* (E1), *Wind event* (W), *Reversal event* (R), *Current event* (C) and *EAC 2* (E2).

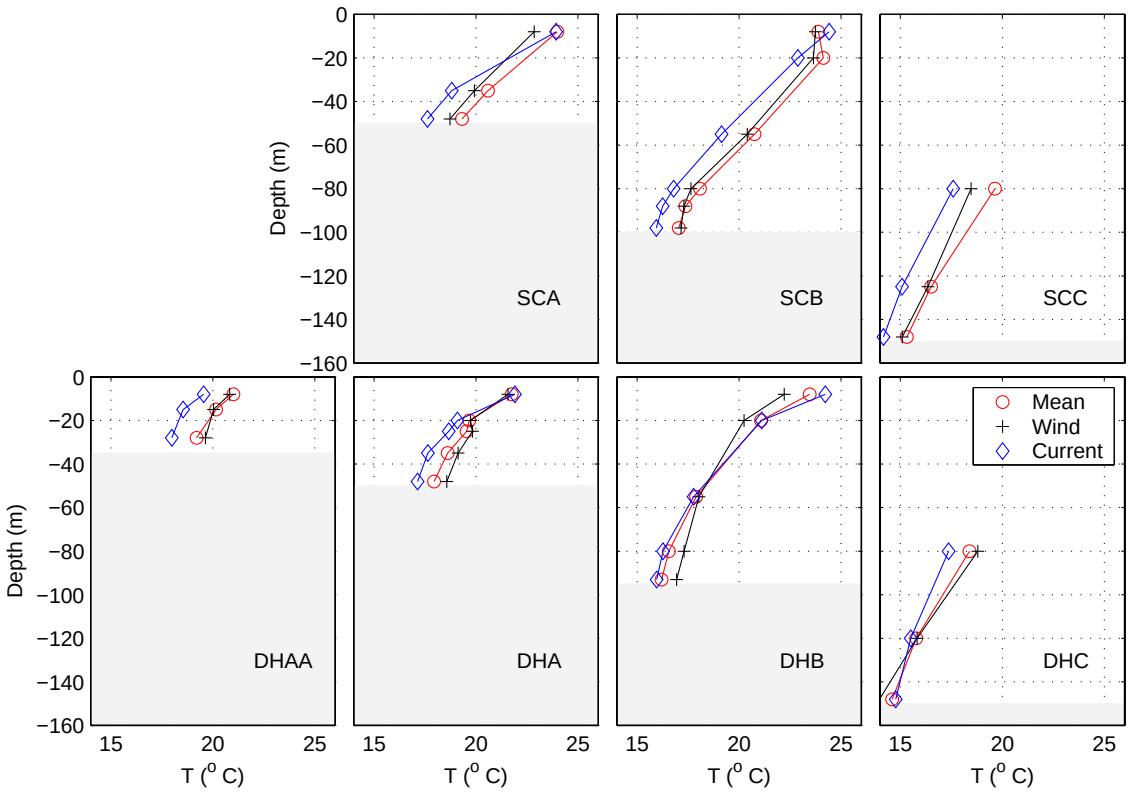

Figure 6: Temporal mean of the temperature time series at the Smoky Cape and Diamond Head moorings and the mean temperature during the *Wind event* and the *Current event*.

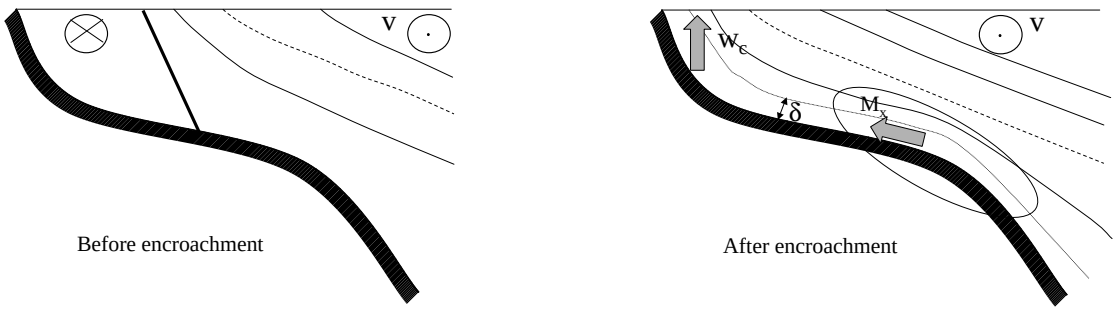

Figure 7: Schematic representation of an alongshore jet before (left) and after encroachment (right) showing how current-driven upwelling occurs in the BBL as the current encroaches upon the coast. The solid lines represent the isotachs of the southward flowing current, where the thick line represents the line of zero velocity, and the dashed line represents the 1 ms^{-1} isotach. In the figure on the right the oval indicates a region of high bottom stress. Also shown are the alongshore current (v), mass transport (M_x) through the BBL of thickness δ and the resultant current-driven uplift (w_c).

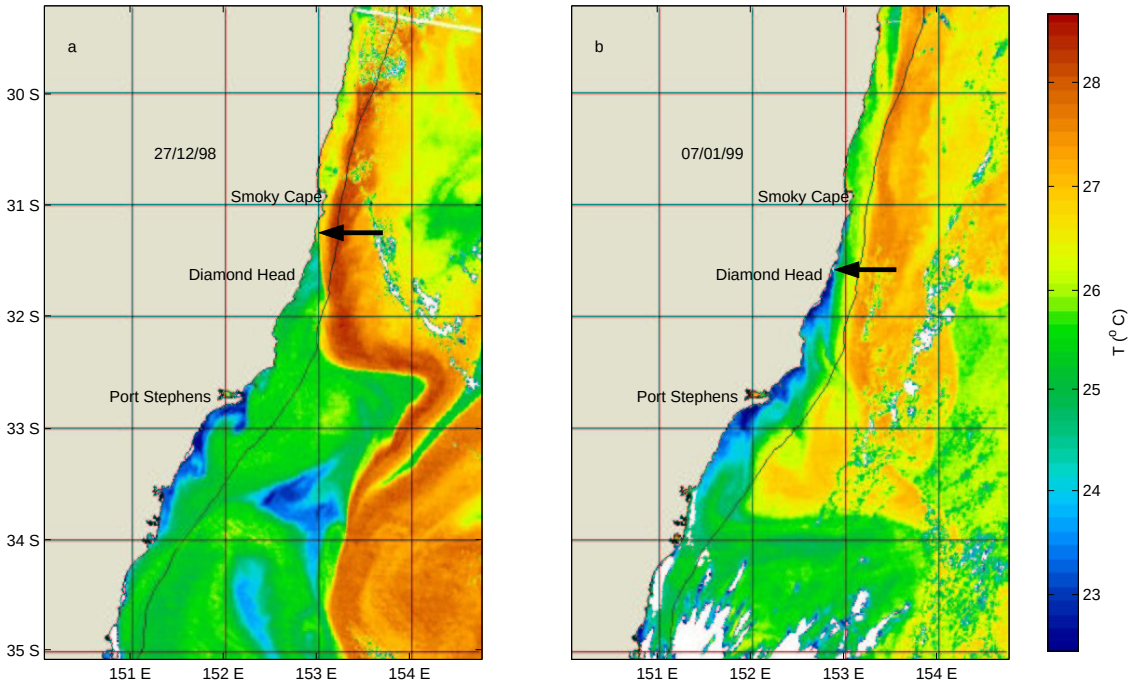

Figure 8: Satellite images of sea surface temperature (°C) on 27 December 1998 (a) and 7 January 1999 (b). The horizontal arrows indicate the position of the EAC separation point and the black line adjacent to the coast represents the 200 m isobath.

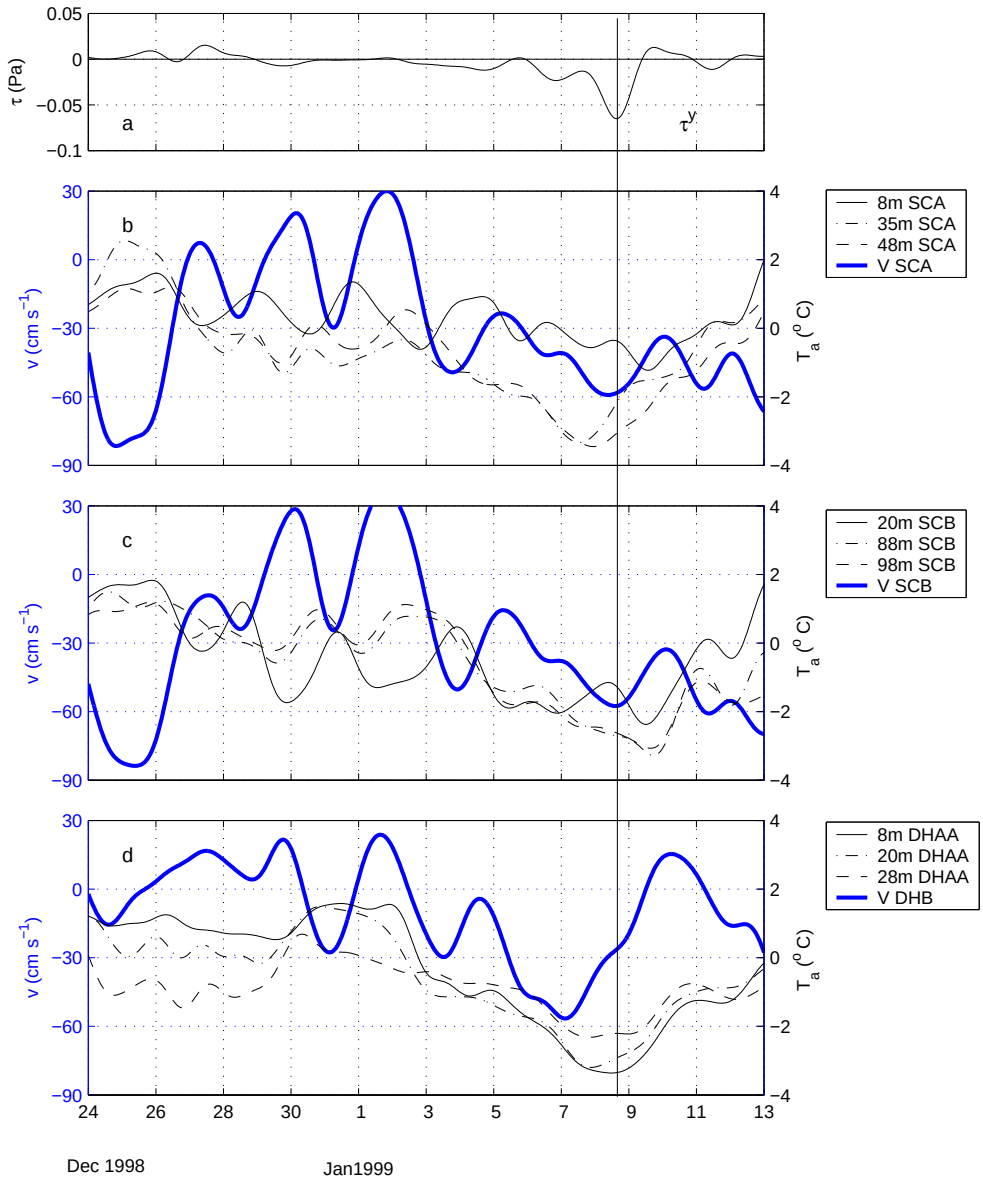

Figure 9: Time series of a) alongshore wind stress (τ^y); b) alongshore depth averaged currents ($\bar{v}$) (bold line) and temperature anomaly (T_a) at SCA; c) $\bar{v}$ and T_a at SCB and d) $\bar{v}$ mid-shelf at DHB and T_a inshore at DHAA during the *Current event*. The thin lines show the temperature at various depths as indicated in the legend of each subplot. The vertical line indicates the timing of the maximum wind stress.

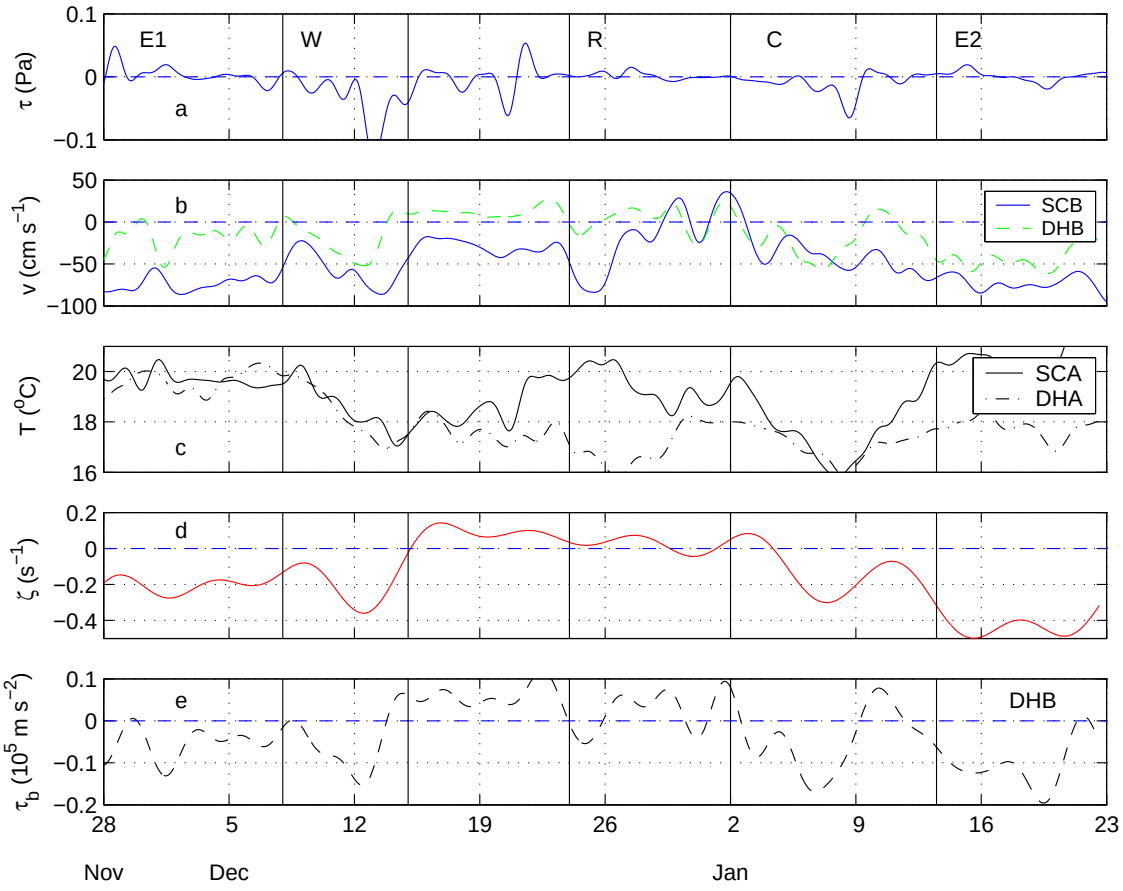

Figure 10: Time series of a) alongshore wind stress (τ^y); b) depth averaged alongshore velocity ($\bar{v}$) at SCB and DHB; c) temperature (T) in the BBL at SCA and DHA; d) depth averaged vorticity (ζ) and e) time series of the alongshore component of bottom stress τ_b.

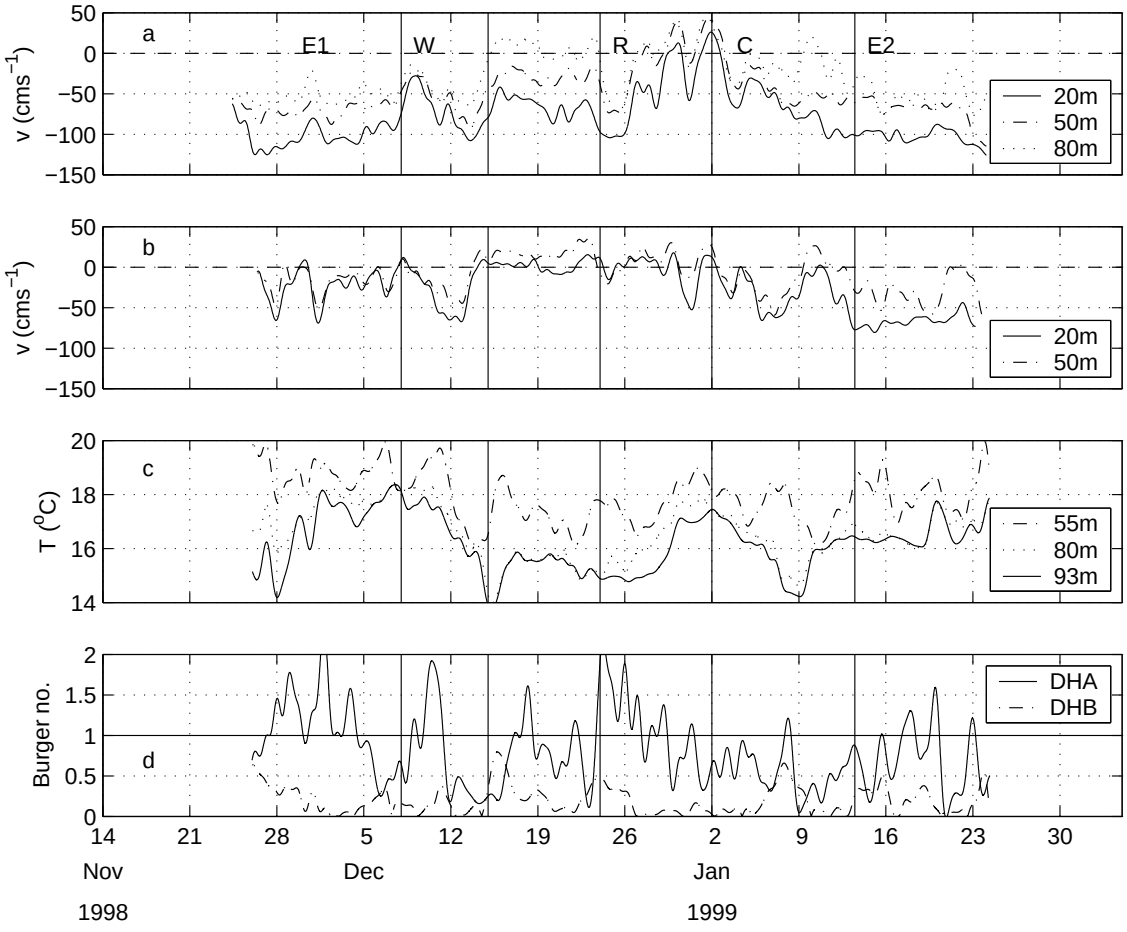

Figure 11: Time series of a) alongshore velocity (v) at SCB; b) alongshore velocity (v) at DHB; c) Temperature (°C) at DHB and d) Burger number (S) at DHA and DHB.